minerals

MDPI

Article

Precambrian Crustal Composition and Reworking in the Western Margin of the Yangtze Craton: Constraints from Sr-Nd-Hf Multi-Isotope Mapping

Xinyue Li [1,2], Wenyan He [1,*], Tingting Feng [2], Huaqing Wang [3], Nan Zhang [2], Hongyi Wu [2] and Bo Zhao [4]

[1] State Key Laboratory of Geological Processes and Mineral Resources, China University of Geosciences, Beijing 100083, China; 15100837639@163.com
[2] Fourth Hydrogeological and Engineering Geological Brigade, Hebei Bureau of Geological Exploration and Mineral Development, Hebei Ground Subsidence Monitoring, Early-Warning and Prevention Center, Cangzhou 061000, China; 13102706355@163.com (T.F.); zhangnan325@163.com (N.Z.); 15530030187@163.com (H.W.)
[3] China Metallurgical Geology Bureau, Beijing 100025, China
[4] No. 6 Geological Team of Shandong Provincial Bureau of Geology and Mineral Resources, Weihai 264209, China; 17853321385@163.com
* Correspondence: wyhe@cugb.edu.cn

Abstract

Regional multi-isotope mapping provides an effective means of investigating deep crustal composition and crustal reworking processes. The western margin of the Yangtze Craton has experienced multiple episodes of magmatism, crustal reworking, and mineralization since its formation, making it an ideal region for exploring the relationship between deep crustal evolution and metallogenic systems. In this study, Sr-Nd-Hf isotopic and whole-rock geochemical mapping was conducted based on compiled geochronological, geochemical, and isotopic datasets, integrated with deep geophysical data, to reconstruct the Precambrian crustal composition and reworking processes of the region. The results reveal significant crustal heterogeneity in the western margin of the Yangtze Craton. West of the Anninghe Fault Zone, rocks exhibit depleted Nd-Hf isotopic signatures ($\varepsilon_{Hf}(t) = 0$ to $+17$; $\varepsilon_{Nd}(t) = 0$ to $+6$), low I_{Sr} values (0.702–0.710), and high Nb/Ta (14–26) and Zr/Hf (36–46) ratios, indicating derivation from the remelting of juvenile mafic lower crust and providing direct evidence for Proterozoic underplating of mantle-derived magmas. In contrast, rocks east of the Anninghe Fault Zone show enriched Nd-Hf isotopic signatures ($\varepsilon_{Nd}(t) = -9$ to 0; $\varepsilon_{Hf}(t) = -7.5$ to 0), higher I_{Sr} values (0.711–0.726), and lower Nb/Ta and Zr/Hf ratios (8–13 and 21–35), suggesting remelting of ancient continental crust. Mineralization is closely associated with crustal architecture. IOCG deposits mainly occur in juvenile crustal domains, whereas Sn polymetallic and phosphate deposits are associated with ancient reworked crust. Under the Precambrian subduction setting, continuous arc magmatism promoted juvenile crust growth, whereas asthenospheric upwelling facilitated ancient crustal reworking, jointly controlling the spatiotemporal distribution of metallogenic systems along the western margin of the Yangtze Craton.

Keywords: isotopic mapping; crustal reworking; Precambrian; Yangtze Craton

Check for updates

Academic Editor: Urs Klötzli

Received: 16 June 2026
Revised: 22 July 2026
Accepted: 23 July 2026
Published: 30 July 2026

Copyright: © 2026 by the authors. Licensee MDPI, Basel, Switzerland. This article is an open access article distributed under the terms and conditions of the Creative Commons Attribution (CC BY) license.

1. Introduction

Igneous rocks are widely distributed, amenable to dating, and can preserve information related to their source regions. Regional isotope mapping of these rocks can reveal the spatial and temporal distribution of various components within the middle–lower crust and lithospheric mantle. In particular, advances in analytical techniques and the accumulation of high-quality data have enabled large-scale isotope mapping in recent years [1–3]. Such mapping, based on extensive Nd and Hf isotopic data from igneous rocks, provides important constraints on deep crustal composition, tectonic boundaries, and crust–mantle interactions, while offering critical insights into continental crust growth and regional tectono-magmatic evolution [4–12].

The Yangtze Craton is one of the three major cratons in East Asia and is located between the Indian, Eurasian, and Pacific plates [13,14]. It has experienced a prolonged and complex geological evolution, with an initial continental nucleus forming in the Hadean (3.8 Ga) and craton stabilization occurring during the Archean–Paleoproterozoic (2.9–1.8 Ga) [15,16]. The western margin of the Yangtze Craton experienced significant crustal growth and reworking during the Precambrian. During the early Precambrian (~1000–780 Ma), subduction-related modification of oceanic crust triggered extensive emplacement of mantle-derived arc magmas, which further modified the juvenile lower crust [17,18]. These ascending magmas transported abundant ore-forming elements, including Fe and Cu, which accumulated at the base of the continental crust and ultimately contributed to the formation of voluminous iron oxide–copper–gold (IOCG) deposits, a distinctive type of hydrothermal deposit enriched in iron oxides [19–21]. During the late Precambrian, mantle convection induced the remelting and reworking of Proterozoic crust [22,23], resulting in the formation of large-scale Sn polymetallic deposits and phosphate mineralization [24–26]. Therefore, the western margin of the Yangtze Craton represents an ideal region for investigating Precambrian multi-isotope signatures, constraining deep crustal composition, and understanding their coupling with metallogenic systems.

Although previous studies and geological projects have generated abundant Sr-Nd-Hf isotopic data and related findings for the western margin of the Yangtze Craton, most investigations have focused on local areas or individual sites [27–30]. Only limited Hf–Nd isotope mapping has been conducted, and regional multi-isotope mapping with integrated constraints remains lacking [31,32]. Based on a systematic compilation of whole-rock geochemical and isotopic datasets across the entire region, this study presents Sr-Nd-Hf multi-isotope and whole-rock geochemical mapping. Combined with the regional tectonic framework, this work provides new insights into deep crustal composition, crustal reworking, and metallogenesis along the western margin of the Yangtze Craton.

2. Geological Background

The earliest continental nucleus of the Yangtze Craton likely formed in the Hadean (3.8 Ga). Following crustal growth during the Meso- to Neoarchean and reworking in the Paleoproterozoic, a stable craton was finally established between 2.9 Ga and 1.8 Ga [15,16]. During the Neoproterozoic (~830 Ma), the Yangtze Craton collided and amalgamated with the Cathaysia Block along the Jiangnan Orogen to form the South China Block (Figure 1a) [33–35]. During the Triassic, the Indosinian orogeny resulted in distinct tectonic boundaries: the northwestern margin of the Yangtze Craton is bounded by the Longmenshan Fault Zone and adjacent to the Songpan–Ganzi Block; its northern margin is connected to the North China Craton via the Qinling–Dabie Oro-

gen; and its southwestern margin adjoins the Indochina Block along the Ailaoshan–Songma Fault [36,37].

The Yangtze Craton is composed of Precambrian crystalline basement and Phanerozoic cover sequences. The basement formed mainly during the Proterozoic, with only minor outcrops of Archean rocks [38,39]. The cover sequences consist mainly of Cambrian to Triassic marine carbonates intercalated with clastic rocks and argillaceous rocks, as well as Jurassic to Quaternary continental sedimentary rocks [40–43]. The Archean Kongling Complex is composed mainly of gneiss, metasedimentary rocks, amphibolite, and granulite; the Paleo- to Mesoproterozoic crystalline basement mainly consists of metasedimentary and metavolcanic rocks, such as the Hekou Group (1.7 Ga) [44], the Dongchuan Group (1742 Ma) [45], and the Dahongshan Group (1711-1659 Ma) [35,46]; the Mesoproterozoic basement is mainly exposed in the Kunyang Group (960 Ma) [47,48], Huili Group (1048–1021 Ma) [49,50], and Julin Group (1050–1043 Ma) [51], with lithologies including metasedimentary rocks, metavolcanic rocks, gneiss, carbonate rocks, as well as A-type dacite, rhyolite, granite, and S-type granite [52,53]; Neoproterozoic strata are mainly represented by the Yanbian Group (1000–865 Ma) in the Panzhihua area, which constitutes a greenschist-facies metamorphic volcano-sedimentary sequence [54–57].

Constrained by the assembly and breakup of the Rodinia supercontinent, the western margin of the Yangtze Craton records multi-stage Precambrian tectonic evolution (Figure 1b). Oceanic slab subduction occurred at ~780–1000 Ma; slab dehydration released fluids that metasomatized the mantle wedge and triggered partial melting, generating voluminous arc magmatic rocks; slab breakoff and enhanced mantle thermal perturbation at ~780–860 Ma induced widespread reworking of Proterozoic crust, coeval with the collision between the Cathaysia Block and Yangtze Craton to form the South China Block. After ~720 Ma, the regional tectonic regime switched to extension, marking the onset of Rodinia breakup [18,37,58]. During this stage, regional tectono-magmatic activity was intense, with widespread intermediate-felsic magmatic rocks and associated minor mafic intrusions [59–61]. These igneous bodies occur between the Anninghe Fault Zone and the Jinhe–Qinghe Fault Zone, trending from north to south. The dominant rock types are granite, diorite, and rhyolite, which provided material sources and host conditions for subsequent regional mineralization [62–64].

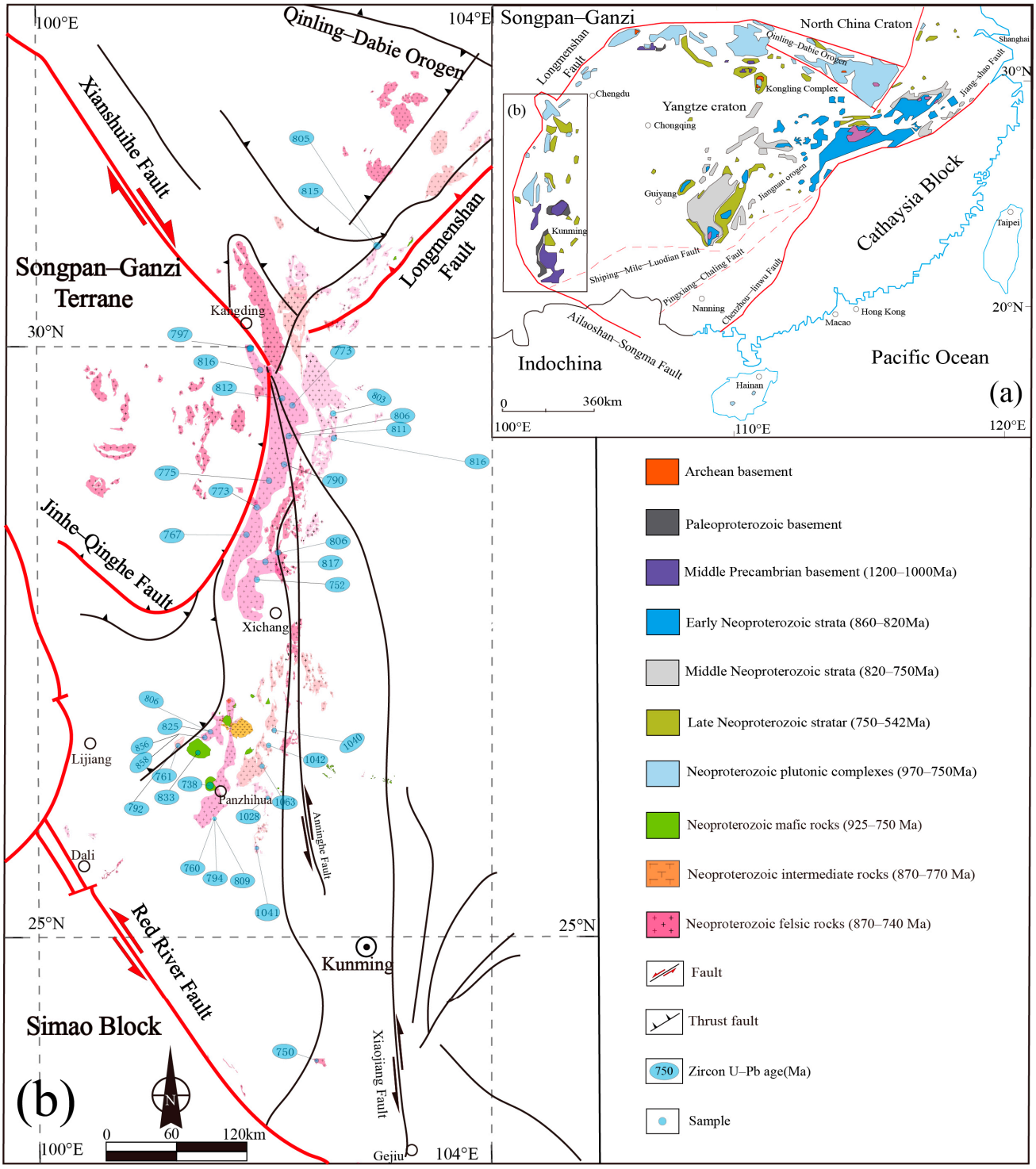


Figure 1. (**a**) Regional geological map of the Yangtze Craton. Modified from [65]. (**b**) Distribution map of igneous rocks in the Western Margin of the Yangtze Craton. Modified after [26].

3. Data Sources and Analytical Results

3.1. Analytical Techniques

Radiogenic Sm-Nd and Lu-Hf isotopes are powerful tracers for distinguishing juvenile crust, reworked crust, depleted mantle and enriched mantle endmembers [27,32]. Sr isotopes, by contrast, can identify crustal contamination during magmatic evolution and serve as a critical complement to the Nd-Hf isotopic systems [4–11]. Combined isotopic mapping and tracing using these three systems avoids the one-sided conclusions derived

from single-isotope analyses [10,32], which is further supported by the robust linear coupling relationships observed in our dataset (Figure 2). Nevertheless, isotopic mapping is inherently limited by the outcrop distribution of plutons; large data gaps commonly exist within the study area, and this approach fails to constrain the vertical lithospheric architecture at depth [10,32]. Geophysical surveys can compensate for this limitation. Accordingly, the integrated application of multiple analytical techniques enables a more comprehensive and precise reconstruction of lithospheric compositional variations and evolutionary history [9,32].

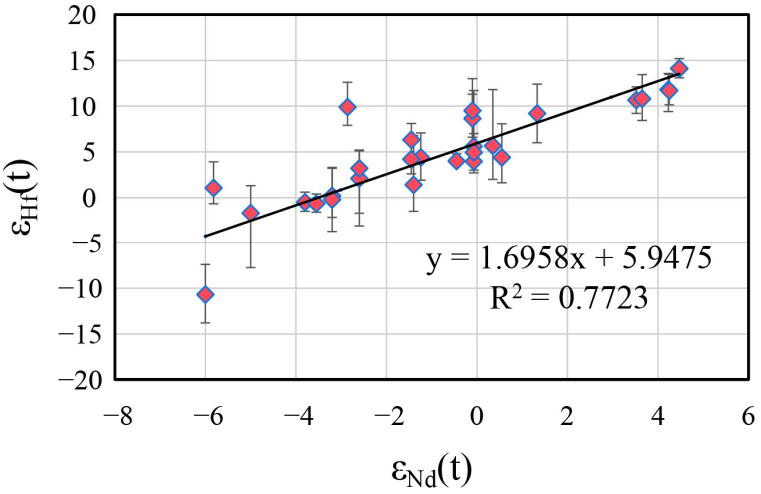


Figure 2. Mapping of whole-rock $\varepsilon_{Nd}(t)$ and zircon $\varepsilon_{Hf}(t)$ in the western margin of the Yangtze Craton. Data sources are from [66–76].

Following the above analytical framework, we systematically compiled all publicly available published datasets from the study area, including zircon U-Pb geochronology, whole-rock geochemistry, and coupled Sr-Nd-Hf isotopic data. To guarantee data quality and regional representativeness, standardized filtering procedures were applied to the raw literature data. Spots with severe alteration, excessive analytical errors, significant Pb loss, and metamorphic origins were discarded [77–83], and only valid data from Precambrian intermediate-felsic magmatic rocks were retained. The curated dataset was spatially gridded in Surfer 16 software via the Kriging interpolation method [10,32]. This algorithm minimizes estimation variance to yield optimal unbiased spatial predictions. The resulting contour maps were further refined and graphically edited using Adobe Illustrator 2020 v24.3.0.569.

3.2. Data Sources

This study integrates published regional data and field geochemical analyses to compile a dataset comprising nearly 80 groups of zircon Hf isotopic analyses, 60 sets of whole-rock Sr-Nd isotopic data, and 50 whole-rock geochemical datasets from Precambrian intermediate-felsic magmatic rocks. Sampling sites cover almost the entire study area, with geographic coordinates of all samples provided in the Supplementary Materials. Confined between the Anninghe Fault Zone and the Jinhe–Qinghe Fault Zone, the magmatic rock bodies crop out discontinuously in a north–south trending belt, with concentrated exposures in the Panzhihua–Xichang (Panxi) region. A diverse suite of lithologies is developed within the study area, including granite, granodiorite, diorite, monzogranite, granite porphyry, syenogranite, biotite granite, rhyolite, quartz diorite, and quartz porphyry. Granitoids account for the largest proportion (63%), followed by dioritic rocks (27%), while rhyolites and porphyries each make up the smallest share (5%). Despite their extensive areal distribution, these rock units exhibit prominent geochemical heterogeneity reflected by major elements, trace elements, and combined Sr-Nd-Hf isotopic signatures.

Major element results indicate that most samples correspond to granite and granodiorite. Their SiO_2 contents vary widely from 57.62 to 77.1 wt.% (Figure 3a), with K_2O/Na_2O ratios ranging between 0.19 and 4.22 (Figure 3c,d). The aluminum saturation index (A/CNK) of the rocks predominantly falls within 1–1.2, classifying them as weakly metaluminous to peraluminous series (Figure 3b). Distinct trace element fractionation is observed in all samples: the vast majority are enriched in light rare earth elements (LREEs) and large-ion lithophile elements (LILEs; e.g., Rb, K, U, Th), alongside relative depletion of high-field-strength elements (HFSEs; e.g., Ti, Nb, P) (Figure 4a,b). Geochronological data (Figure 5) show that the sample ages range from 1168–616 Ma. The zircon Hf and whole-rock Sr–Nd isotopic compositions display extremely wide variation ranges (Figure 6a,c), with $\varepsilon_{Hf}(t)$ values of −9 to +17, $\varepsilon_{Nd}(t)$ values of −7.5 to +6.0, and initial $^{87}Sr/^{86}Sr$ ratios (I_{Sr}) ranging from 0.702 to 0.726.

Collectively, these lines of evidence verify intense compositional heterogeneity of Precambrian intermediate-felsic magmatic rocks along the western margin of the Yangtze Craton. This heterogeneity points to remarkable compositional variability in the parental magma sources and records multistage complex magmatic processes, including variable degrees of partial melting, fractional crystallization, and crust–mantle mixing during magmatic evolution [26].

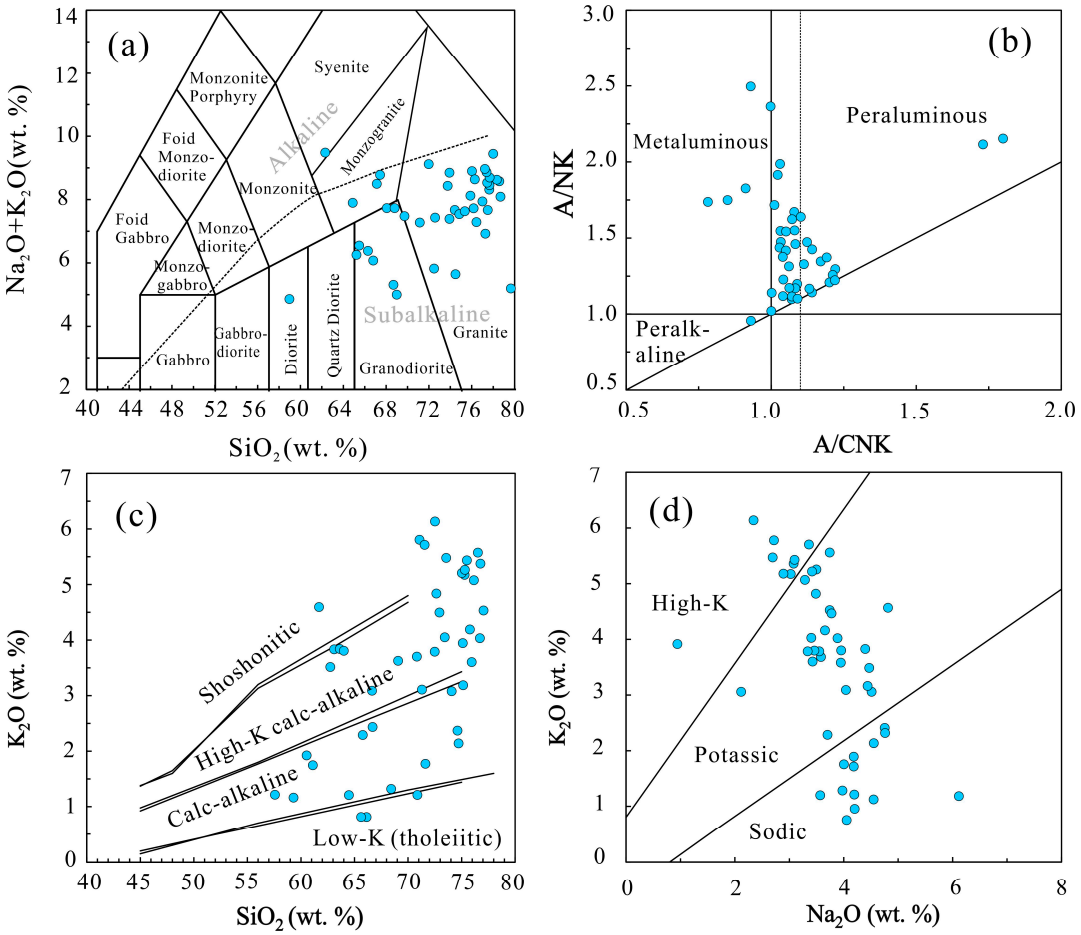


Figure 3. (**a**) Total Alkali–Silica (TAS) diagram. The dashed line marks the boundary between the alkaline and subalkaline series. (**b**) A/NK versus A/CNK diagram. The vertical dashed lines denote A/CNK = 1.0 and 1.1, with the interval between them representing the weakly peraluminous field. (**c**) K_2O versus SiO_2 diagram. (**d**) K_2O versus Na_2O diagram [66–76].

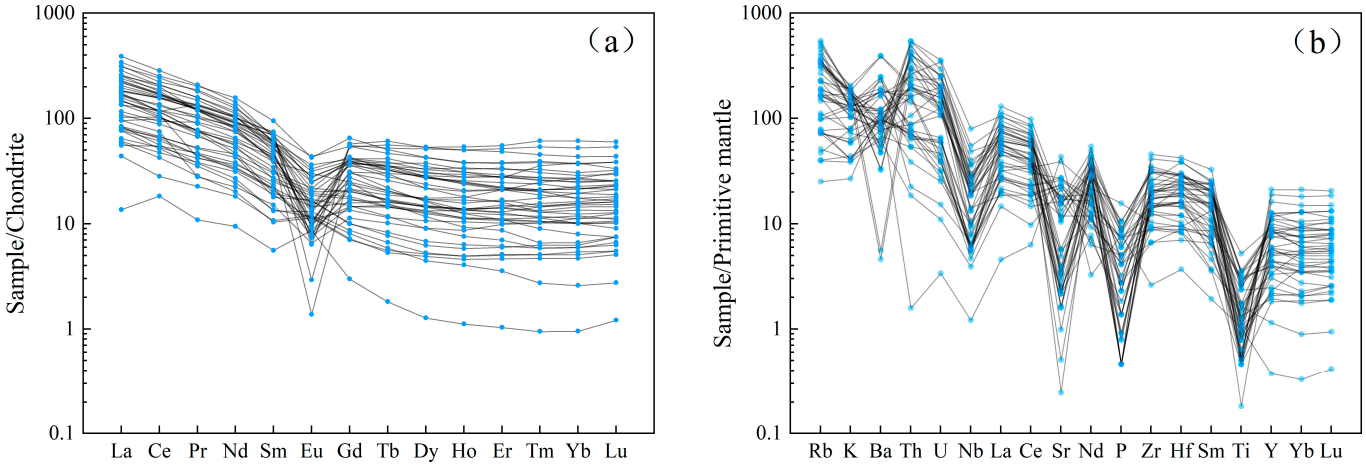


Figure 4. (**a**) Chondrite-normalized REE patterns; (**b**) Primitive mantle-normalized trace-element patterns [66–76].

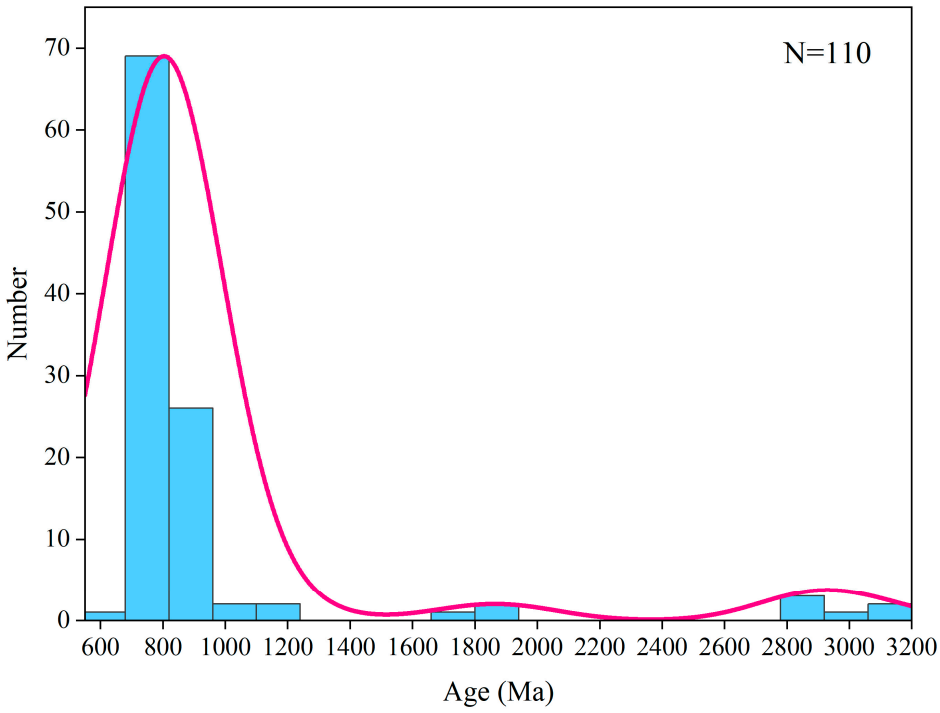


Figure 5. Zircon age spectra of intermediate-felsic magmatic rocks in the western margin of the Yangtze Craton. Data sources are from [66–76].

3.3. Analytical Results

This study compiled geological, geochronological, and isotopic geochemical data for intermediate-felsic igneous rocks in the study area. Geochronological results indicate that Precambrian magmatic rocks in the region are dominated by granite and diorite assemblages (Figure 1), with emplacement ages mainly ranging from 1168 to 616 Ma. Magmatic activity was weak before 1700 Ma, with only sporadic records between 3092 and 1764 Ma (Figure 5). Zircon $\varepsilon_{Hf}(t)$ values of magmatic rocks from the study area exhibit a wide range (−10.7 to +15.2), with most values being positive and an average of +4.4 (Figure 6a). The Hf isotopic compositions mostly plot along the evolution line of Proterozoic granite zircons, with only a few falling on the evolution line of Archean metamorphic basement zircons (Figure 6c). The two-stage Hf model ages range from 3419 Ma to 780 Ma, with a peak between 1800 Ma and 800 Ma (Figure 6b). Whole-rock Sr–Nd isotopic compositions are heterogeneous. $\varepsilon_{Nd}(t)$ values

vary from −7 to +6.3, and initial $(^{87}Sr/^{86}Sr)_i$ ratios range from 0.703 to 0.727. Most samples from the study area fall in the juvenile lower crust field, with a minority plotting in the ancient mature crust field (Figure 6d).

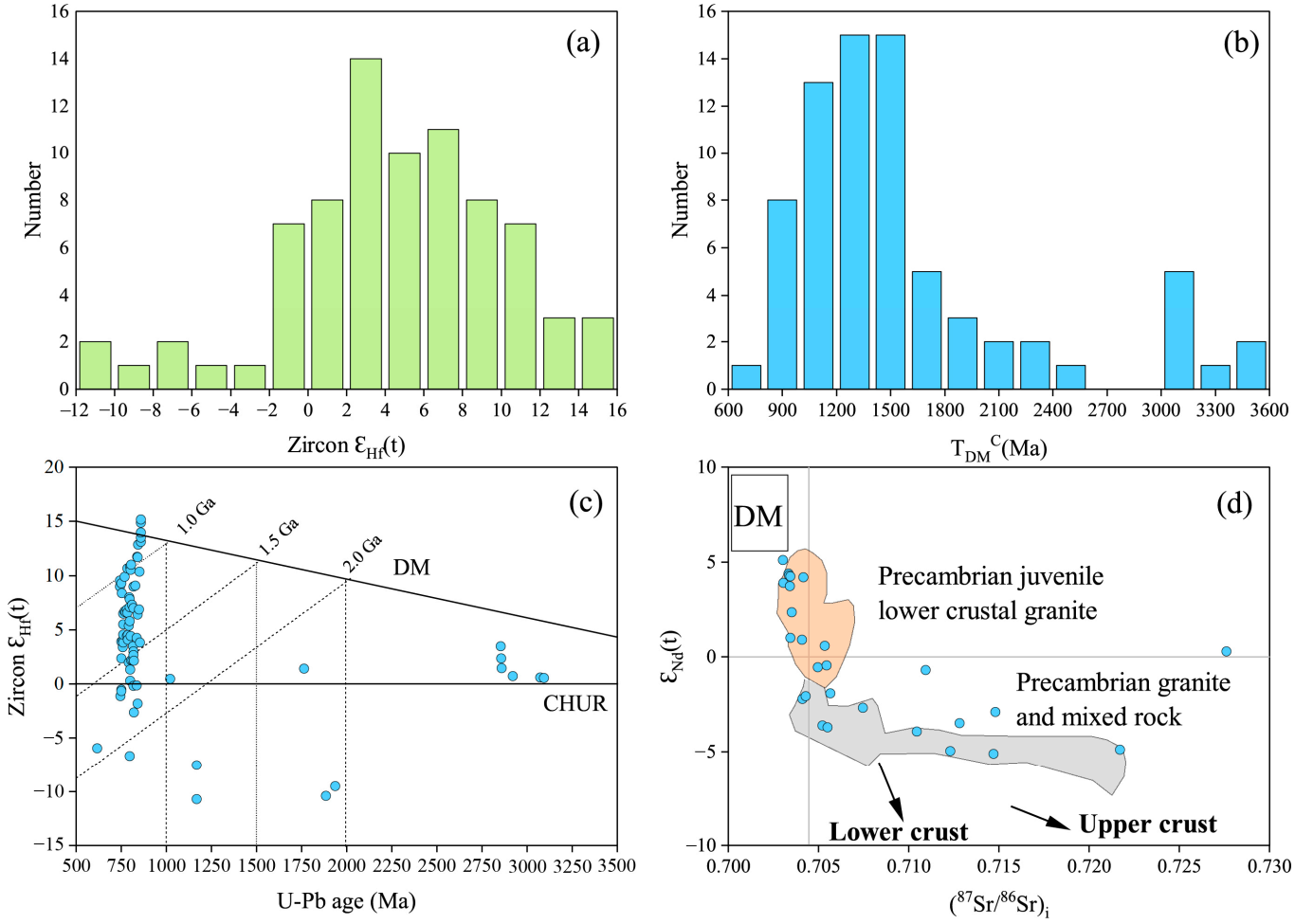


Figure 6. (**a**) Histogram of zircon $\varepsilon_{Hf}(t)$ values. (**b**) Histogram of Hf model ages. (**c**) Plot of zircon $\varepsilon_{Hf}(t)$ versus age. (**d**) Diagram of $\varepsilon_{Nd}(t)$ versus $(^{87}Sr/^{86}Sr)_i$. Data sources are from [66–76].

4. Discussion

4.1. Spatio-Temporal Evolution of Regional Magma

Detailed geochronological investigations reveal extensive Precambrian magmatism along the western Yangtze Craton. These magmatic events predominantly occurred during the Mesoproterozoic to Neoproterozoic, with only sporadic Archean–Paleoproterozoic intrusions exposed [39]. Zircon U-Pb dating yields crystallization ages ranging from 3092 Ma to 616 Ma for magmatic rocks in the study area, with a prominent age peak between 1168 Ma and 616 Ma (Figure 5). In terms of regional tectonic evolution, the embryonic Anninghe Fault Zone developed during the Jinningian Orogeny (ca. 700–1000 Ma). As a long-lived lithospheric weak zone within the western Yangtze basement, this fault exerted persistent control over magma migration and emplacement.

Temporal–spatial magmatic evolution demonstrates that early magmatic activities were concentrated in central Yunnan along the Anninghe Fault, dominated by granitic intrusions. With continuous tectonic reactivation of the fault, late-stage magmatism shifted to the Panxi segment in the central study area, where voluminous granites and diorites were emplaced, alongside minor porphyries and rhyolites [26].

4.2. Crustal Material Composition and Reworking

4.2.1. Source Characteristics

Sr-Nd-Hf multi-isotope analysis is an effective method for tracing the sources of magmatic rocks. Whole-rock Sr and Nd isotopes are generally used together to characterize source regions. However, whole-rock Nd isotopes tend to record more enriched compositions and older model ages compared with zircon Hf isotopes. Additionally, the whole-rock Sr isotopic system is susceptible to modification by magmatic differentiation and fluid-related processes, commonly resulting in anomalous values. Zircon Hf isotopes are more stable and insensitive to the in situ decay of radioactive hafnium [80,84–87], yet zircon Hf isotopic data can be affected by analytical artifacts and may lose signatures of ancient components, leading to decoupling between zircon Hf and whole-rock Nd isotopes. Therefore, a combined Sr-Nd-Hf isotopic approach provides a more robust constraint on the nature of magma sources [31,32].

As outlined above, Precambrian intermediate–felsic rocks on the western Yangtze Craton record crystallization ages ranging from 3092 Ma to 616 Ma(Figure 5). Most samples belong to granite–diorite suites (Figure 3a) and plot as weakly metaluminous to peraluminous lithologies (Figure 3b). The majority of specimens are enriched in light rare earth elements (LREEs) and large-ion lithophile elements (LILEs) including Rb, K, U and Th, while showing depletion in high-field-strength elements (HFSEs) such as Ti, Nb and P, which represents typical crustal geochemical signatures (Figure 4). Zircon $\varepsilon_{Hf}(t)$ values are predominantly positive and mantle-like, varying from 0 to +15 (Figure 6a), and most data points cluster along the 1.0–1.5 Ga evolutionary trend (Figure 6c). Corresponding two-stage Hf model ages are concentrated between 1800 Ma and 800 Ma (Figure 6b), implying crustal growth driven by mantle-derived magma underplating during the Precambrian. On whole-rock Sr-Nd isotopic diagrams, samples mostly fall within the field of juvenile lower crust, characterized by moderately high $\varepsilon_{Nd}(t)$ values (−2 to +5) and low initial $^{87}Sr/^{86}Sr$ ratios (0.703–0.706; Figure 6d). Combined isotopic evidence collectively indicates that primary magmas were mainly sourced from juvenile mafic lower crust. A small subset of samples displays enriched Sr-Nd-Hf isotopic compositions, consistent with partial melting of ancient crustal materials. Samples plot across both adakite and arc magma fields in Figure 7a,b, with the overwhelming majority projecting within the arc magma domain. This feature substantiates prolonged subduction of a Neoproterozoic oceanic slab beneath the primitive mantle wedge during ca. 1000–780 Ma. Fluids released from the subducting slab progressively metasomatized the overlying mantle wedge, whereas the continued injection of arc magmas heated the continental crust over an extended period, resulting in crustal growth and remelting of pre-existing ancient crustal components.

4.2.2. Crustal Composition and Architecture

Taking the western margin of the Yangtze Craton (the study area, Figure 1) as an example, this study conducted multi-isotope mapping of Sr-Nd-Hf isotopes (Figure 8) and Nb/Ta vs. Zr/Hf ratio mapping (Figure 9) for Precambrian intermediate-felsic magmatic rocks. From the perspective of Sr-Nd-Hf isotopic mapping, the crustal material composition and properties in the study area are heterogeneous, with the Anninghe Fault Zone serving as the dividing line: the western part is dominated by juvenile crust, while the eastern part is composed of ancient crust. Zircon Hf isotopes in the western part of the study area are generally characterized by high positive values ($\varepsilon_{Hf}(t)$ = 0 to +17). Combined with the whole-rock Sr–Nd isotopic characteristics ($\varepsilon_{Nd}(t)$ = 0 to +6, $(^{87}Sr/^{86}Sr)_i$ = 0.702–0.710), this indicates that the deep material may have been derived from partial melting of the thickened lower crust (e.g., juvenile or reactivated young crust). In contrast, the isotopic compositions in the eastern part of the study area are characterized by significantly low

$\varepsilon_{Hf}(t)$, low $\varepsilon_{Nd}(t)$, and high initial Sr ratios (I_{Sr}), with $\varepsilon_{Hf}(t)$ ranging from −9 to 0, $\varepsilon_{Nd}(t)$ from −7.5 to 0, and $(^{87}Sr/^{86}Sr)_i$ from 0.711 to 0.726, indicating that the crust is dominated by ancient crustal materials [26].

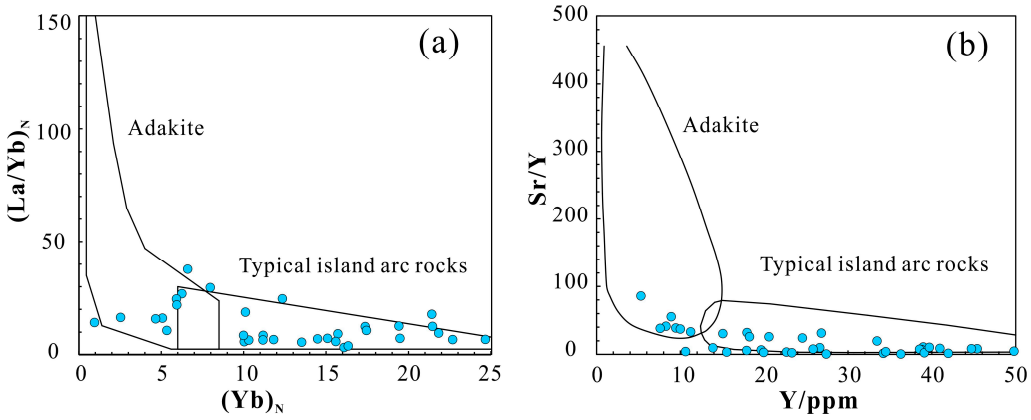


Figure 7. (**a**) Diagram of $(La/Yb)_N$ versus $(Yb)_N$. (**b**) Diagram of Sr/Y versus Y [66–76].

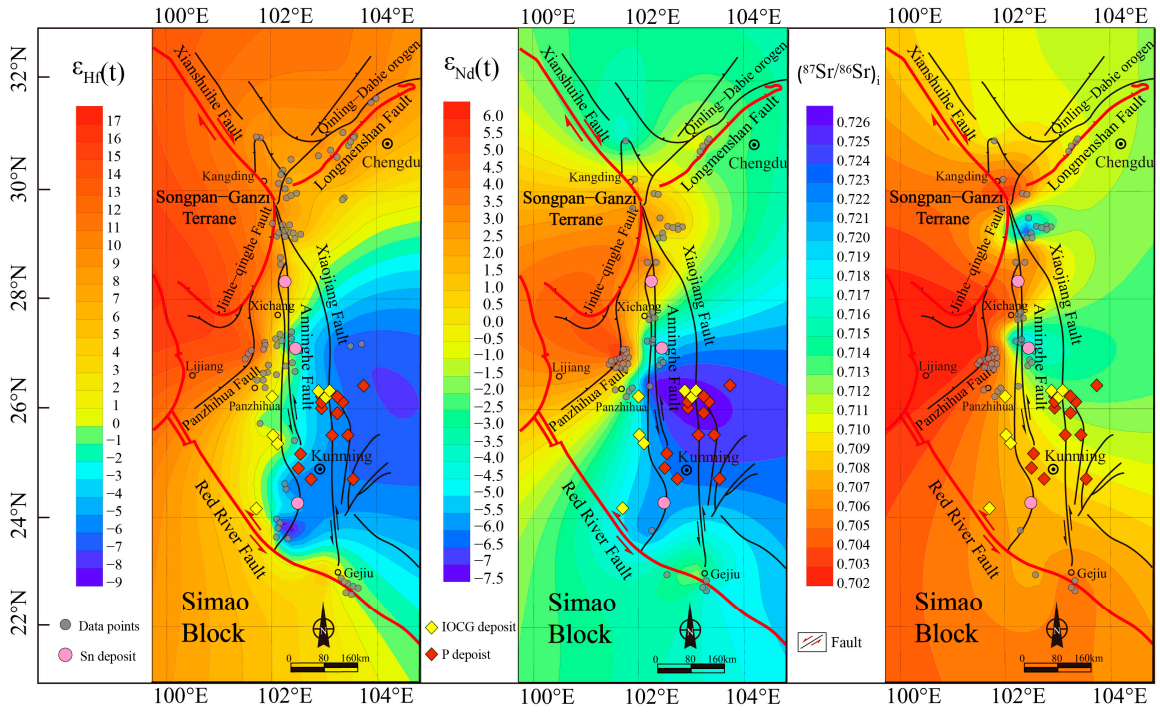


Figure 8. Contour maps of Sr-Nd-Hf isotopes for intermediate-felsic magmatic rocks in the western margin of the Yangtze Craton. Data sources are from [66–76].

As high-field-strength elements (HFSEs), Nb, Ta, Zr, and Hf exhibit strong inertness and similar incompatible characteristics, remaining largely unaffected during magma formation. Thus, Nb/Ta and Zr/Hf ratios can be used to trace the components of the source crust [88]. During crust−mantle differentiation, Ta is significantly enriched while Nb is depleted in the crust: the Nb/Ta ratio of crust-derived magmas ranges from 11 to 12, whereas that of mantle-derived magmas is close to 17.5. The Zr/Hf ratio is 11 for the continental crust, 18.75 for the lower crust, and 36.25 for the primitive mantle. Contour maps of Nb/Ta and Zr/Hf ratios are shown in Figure 9. West of the Anninghe Fault Zone, relatively high Nb/Ta and Zr/Hf ratios are observed (Nb/Ta = 14~26, Zr/Hf = 36~46), which are more similar to those of mantle-derived magmas, indicating a mantle or juvenile crustal source. East of the Anninghe

Fault Zone, the Nb/Ta ratio ranges from 8 to 13 and the Zr/Hf ratio ranges from 21 to 35, indicating the involvement of ancient crustal materials [26].

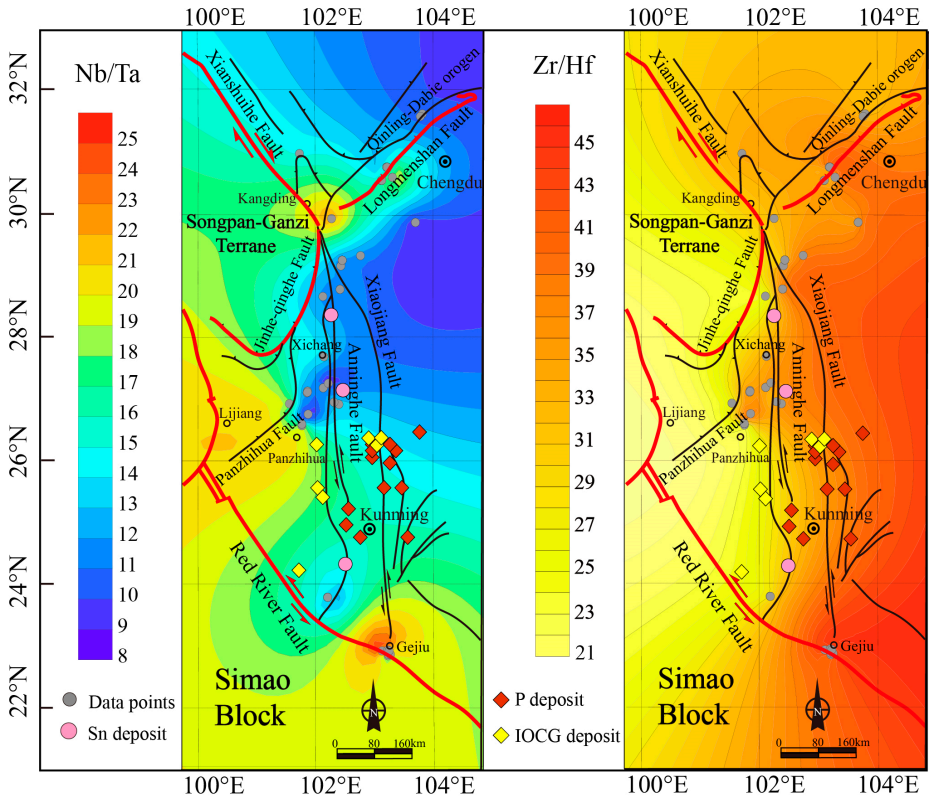


Figure 9. Contour maps of Nb/Ta and Zr/Hf ratios for intermediate-felsic magmatic rocks in the western margin of the Yangtze Craton. Data sources are from [66–76].

Combined with geophysical exploration results (Figure 10), the Moho depth shallows from west to east along the profile, and the crustal thickness shows a thinning trend (approximately 30–45 km) in the western margin of the Yangtze Craton. This indicates the coexistence of ancient and juvenile lithospheres in the study area [89,90], with the western part being a thickened juvenile lower crust and the eastern part being an area reworked by remelting of ancient crust.

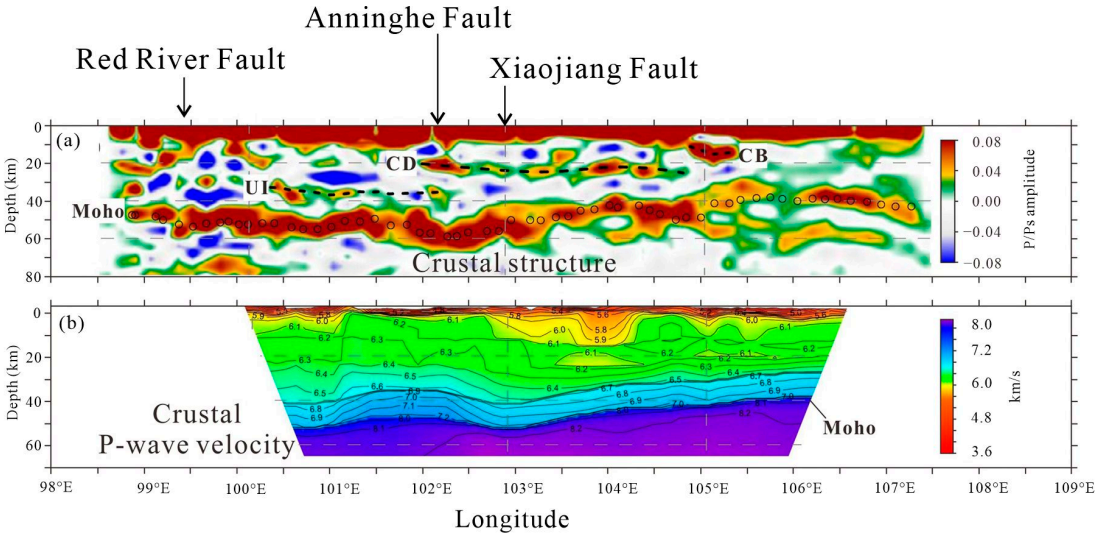


Figure 10. Crustal structure inversion results of the western margin of the Yangtze Craton [89,90].

In summary, the crustal composition of the western margin of the Yangtze Craton is heterogeneous. West of the Anninghe Fault Zone, the crust has gradually accreted and thickened with the injection of mantle-derived arc magmas. In contrast, the ancient reworked crust east of the Anninghe Fault Zone exhibits a thinning structural feature due to lithospheric extension.

4.2.3. Crustal Growth and Reworking

Previous studies suggest that investigating continental growth and reworking events is crucial for understanding crustal formation and evolution, geodynamic mechanisms, and plate tectonic processes [91,92]. Continental crustal growth (including lateral accretion and vertical growth) is mainly achieved through arc-continent collision and rift-related magmatism [16,93]. Its material sources are dominated by mantle-derived components, characterized by highly positive $\varepsilon_{Hf}(t)$ and $\varepsilon_{Nd}(t)$ values, relatively young two-stage model ages, and isotopic compositions close to the depleted mantle evolution line [94]; crustal recycling refers to the process by which crustal materials return to the mantle through subduction, delamination, and other mechanisms, subsequently re-participating in crustal formation, with isotopic compositions showing mixed mantle–crust characteristics [95,96]; crustal reworking involves the remelting and transformation of pre-existing crustal materials, with insignificant contribution from mantle-derived sources. It is characterized by predominantly negative $\varepsilon_{Hf}(t)$ and $\varepsilon_{Nd}(t)$ values, older model ages, and geochemical features plotting entirely within the ancient crustal field [97,98].

Spatially, west of the Anninghe Fault Zone, a red–yellow area with high $\varepsilon_{Hf}(t)$, high $\varepsilon_{Nd}(t)$, and low initial Sr ratios (I_{Sr}) is formed, indicating that the magmas are products of partial melting of a metasomatized mantle wedge. The Nb/Ta and Zr/Hf ratios are generally high, reflecting the injection of a large amount of juvenile mantle-derived materials, which has made an important contribution to crustal growth. In contrast, east of the Anninghe Fault Zone in the study area, the magmas are characterized by low negative $\varepsilon_{Hf}(t)$ and $\varepsilon_{Nd}(t)$ values, as well as high I_{Sr} values, indicating that the magma source is the remelting of ancient crust. Their low Nb/Ta and Zr/Hf ratios suggest that the magma source is mainly at a deep crustal scale, representing a typical crustal reworking domain.

Overall, the Precambrian evolution of the western Yangtze Craton records two coupled geological processes: juvenile crustal growth and reworking of ancient crust. Continuous remelting and modification of Archean–Proterozoic continental crust took place throughout this period [16,17]. During the assembly of the Rodinia supercontinent, southward and northward subduction beneath the Yangtze Block separately generated two island–arc systems, namely the Xixiang Arc and Shuangxiwu Arc (Figure 11). In the early subduction stage, fluids released from the subducted oceanic slab metasomatized the overlying mantle wedge and produced arc magmas, which promoted lateral crustal growth. Mixing of juvenile mantle-derived components with pre-existing basement rocks simultaneously triggered crustal reworking [99,100]. The early granites in central Yunnan represent the magmatic products of lateral crustal growth related to the southern Shuangxiwu Arc. Slab breakoff occurred in the late subduction stage and triggered asthenospheric upwelling. Mantle-derived mafic magmas underplated the lower crust and resulted in vertical crustal growth [91,92], which corresponds to voluminous granodiorite magmatism across the Panxi region. Nevertheless, late-stage extensional tectonism and erosion partially counterbalanced previous crustal growth, eventually forming a crustal architecture thicker in the west and thinner in the east. The Jinningian Anninghe Fault acted as a vertical conduit for deep melt migration, governing the spatial zoning of magmas from the northern and southern arc systems. This tectonic framework fully accounts for the concentrated distribution of Mesoproterozoic–Neoproterozoic arc magmatic rocks within the study area [16,17].

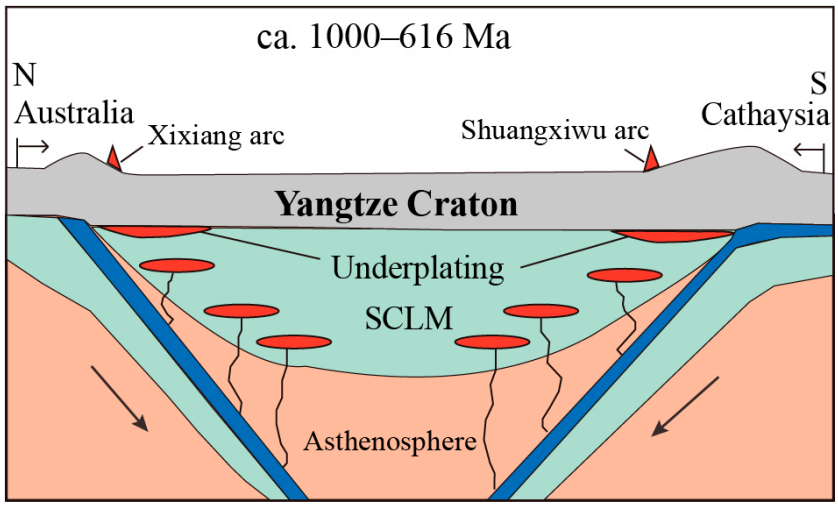


Figure 11. Tectonic evolution model of the western margin of the Yangtze Craton [21].

4.3. Coupling Relationship Between Crustal Properties and Mineralization

The temporal and spatial distribution of ore deposits in the study area is jointly controlled by regional crustal properties and deep fault systems.

Temporally, all deposits within the study area formed between 1083 Ma and 521.9 Ma, nearly synchronously with or slightly postdating regional magmatism (1168–616 Ma). Spatially, iron oxide–copper–gold (IOCG) deposits are predominantly developed on the western side of the Anninghe Fault Zone [101,102]. Host rocks exhibit high $\varepsilon_{Hf}(t)$, high $\varepsilon_{Nd}(t)$ and low initial $^{87}Sr/^{86}Sr$ (I_{Sr}) isotopic signatures, coupled with elevated Nb/Ta and Zr/Hf ratios. Geochemical discrimination diagrams (Sr/Y, V/Sc, 10,000 × δEu/Y) yield Sr/Y > 20, V/Sc > 5 and 10,000 × δEu/Y > 500, recording melting signals derived from juvenile thickened lower crust formed in a subduction setting (Figure 12). During Neoproterozoic fault reactivation, slab-derived ore-bearing fluids migrated upward along major faults and secondary fractures. Large-scale fluid exsolution occurred at the base of the crust, triggering enrichment and mineralization of Cu and Au [103]. By contrast, Sn-polymetallic and phosphate deposits are mainly exposed east of the Anninghe Fault. Their host rocks are characterized by low $\varepsilon_{Hf}(t)$ low $\varepsilon_{Nd}(t)$, and high I_{Sr} values, together with geochemical indices of Sr/Y < 20, V/Sc < 3 and 10,000 × δEu/Y < 500 (Figure 12), indicative of partial melting of reworked ancient crust. Fault activation drove deep heat conduction, which induced remelting and metamorphic differentiation within the ancient middle–lower crust east of the fault. Sn and P elements were mobilized and extracted by crust-derived fluids, before final shallow emplacement along interlayer fracture zones and intrusive contact margins to form ore bodies [26].

In summary, crustal architecture and metallogenic characteristics across the western Yangtze Craton exhibit distinct lateral differentiation. Moving eastward across the Anninghe Fault Zone, crustal nature transitions progressively from juvenile crust to reworked ancient crust, accompanied by a shift in deposit types from IOCG mineralization to Sn-polymetallic and phosphate mineralization [101,102]. Two major episodes of tectonic activity are recorded along the Anninghe Fault Zone. During the Jinningian period (700–1000 Ma, coeval with Rodinia supercontinent assembly), the embryonic fault formed and underwent its first major tectonic movement, acting as a fundamental lithospheric weak zone generated under the bidirectional subduction of the northern Xixiang Arc and southern Shuangxiwu Arc of the Yangtze Craton (Figure 11). In the middle Neoproterozoic (616–850 Ma), slab rollback and extensive asthenospheric underplating triggered cratonic reworking, leading to intense reactivation of this fault. During fault reactivation, deep

crust–mantle ore-bearing fluids migrated upward for long distances along fault conduits. The juvenile thickened lower crust on the western side melted under the influence of mantle-derived fluids, generating IOCG deposits. Fluid heat propagated eastward and induced remelting and metamorphic differentiation within the Archean–Paleoproterozoic ancient lower crust in the eastern domain, mobilizing Sn and P metallogenic elements and eventually concentrating them to form tin-phosphate deposits.

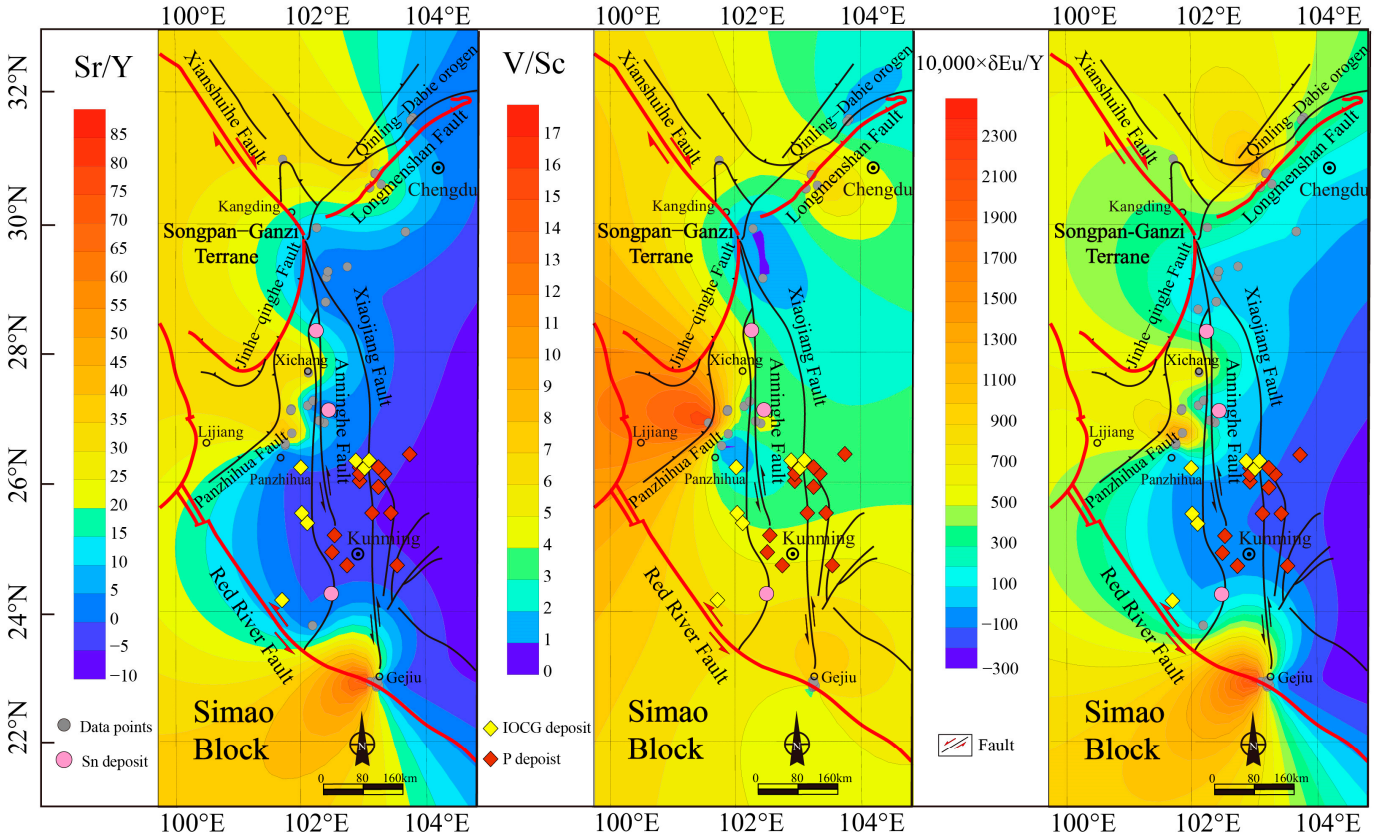


Figure 12. Contour maps of Sr/Y, V/Sc and 10,000 × δEu/Y ratios for intermediate-felsic magmatic rocks in the western margin of the Yangtze Craton. Data sources are from [66–76].

It is therefore concluded that the two-stage tectonic evolution of the fault exerts rigorous controls on regional crustal differentiation, magmatism, and the spatial distribution and genetic types of mineral deposits [23,92].

5. Conclusions

Based on Sr-Nd-Hf isotopic and whole-rock geochemical mapping of intermediate-felsic igneous rocks in the western margin of the Yangtze Craton, this study draws the following conclusions:

1. Precambrian magmatism (3092–616 Ma) in the study area is mainly distributed along the Anninghe Fault Zone, with granites and dioritic rocks as the dominant lithologies. The geochemical characteristics can be divided into two groups. One group is characterized by positive $\varepsilon_{Hf}(t)$ and $\varepsilon_{Nd}(t)$ values, low initial Sr isotope ratios (I_{Sr}), and high Nb/Ta and Zr/Hf ratios, representing juvenile crustal growth. The other group exhibits negative $\varepsilon_{Hf}(t)$ and $\varepsilon_{Nd}(t)$ values, high I_{Sr} values, and low Nb/Ta and Zr/Hf ratios, corresponding to ancient crustal reworking domains.
2. With oceanic plate subduction and the continuous emplacement of mantle-derived arc magmas, the composition of crustal materials evolved progressively. The western side of the Anninghe Fault Zone experienced significant crustal accretion and thickening

during the early Precambrian, resulting in the formation of a juvenile crustal domain. In contrast, the eastern side represents an ancient reworked crustal domain. During the late Precambrian, rollback and break-off of the subducting slab hindered continued crustal accretion and thickening, leading to crustal thinning in this region.

3. Mineralization in the study area is closely associated with crustal composition and architecture. Most IOCG deposits occur within the juvenile crustal domain, whereas Sn polymetallic deposits and phosphate deposits are mainly developed in ancient reworked crustal domains.

Supplementary Materials: The following supporting information can be downloaded at: https://www.mdpi.com/article/10.3390/min16080797/s1, Table S1: Summary of Hf isotopic data of zircons in the Western Margin of the Yangtze Craton; Table S2: Summary of Whole-rock Sr-Nd isotopic compositions data in the Western Margin of the Yangtze Craton; Table S3: Summary of whole-rock geochemical data in the Western Margin of the Yangtze Craton.

Author Contributions: Conceptualization, X.L.; methodology, W.H. and X.L.; software, X.L., T.F. and N.Z.; validation, X.L. and W.H.; formal analysis, X.L., W.H., H.W. (Huaqing Wang), N.Z. and H.W. (Hongyi Wu); investigation, X.L., B.Z. and W.H.; resources, X.L., H.W. (Hongyi Wu) and T.F.; data curation, B.Z. and X.L.; writing–original draft preparation, X.L.; writing–review and editing, X.L., W.H., B.Z. and T.F.; visualization, X.L., H.W. (Huaqing Wang) and N.Z.; supervision, W.H. and T.F.; project administration, W.H.; funding acquisition, W.H. All authors have read and agreed to the published version of the manuscript.

Funding: This research was funded by the National Natural Science Foundation of China (Grant No. 42372098, U2444212) and the Heilongjiang Provincial Natural Science Foundation of China (Grant No. LH2024d027).

Data Availability Statement: Raw data are provided within the Supplementary Materials of this article.

Conflicts of Interest: Xinyue Li, Tingting Feng, Nan Zhang and Hongyi Wu are employed by Fourth Hydrogeological and Engineering Geological Brigade, Hebei Bureau of Geological Exploration and Mineral Development; Huaqing Wang is employed by China Metallurgical Geology Bureau; Bo Zhao is employed by No. 6 Geological Team of Shandong Provincial Bureau of Geology and Mineral Resources. The paper re-flects the views of the scientists and not the company.

References

1. Wang, T.; Hou, Z.Q. Isotopic Mapping and Deep Material Exploration (I): Revealing Lithospheric Compositional Evolution and Crustal Growth. *Earth Sci. Front.* **2018**, *25*, 1–19. (In Chinese) [CrossRef]
2. Hou, Z.Q.; Wang, T. Isotopic Mapping and Deep Material Exploration (II): Imaging Crustal 3D Architecture and Regional Metallogenic Regularities. *Earth Sci. Front.* **2018**, *25*, 20–41. (In Chinese) [CrossRef]
3. Mo, X.X. Growth and evolution of the Tibetan Plateau crust from magmatic rocks. *Earth Sci. Front.* **2020**, *45*, 2245–2257. (In Chinese) [CrossRef]
4. Champion, D.C.; Cassidy, K.F. An overview of the Yilgarn Craton and its crustal evolution. *Geosci. Aust. Rec.* **2007**, *14*, 8–13.
5. Wang, T.; Jahn, B.M.; Kovach, V.P.; Tong, Y.; Hong, D.W.; Han, B.F. Nd–Sr isotopic mapping of the Chinese Altai and implications for continental growth in the Central Asian Orogenic Belt. *Lithos* **2009**, *110*, 359–372. [CrossRef]
6. Dickin, A.; Herrell, M.; Moore, E.; Cooper, D.; Pearson, S. Nd isotope mapping of allochthonous Grenvillian klippen: Evidence for widespread 'ramp-flat' thrust geometry in the SW Grenville Province. *Precambrian Res.* **2014**, *246*, 268–280. [CrossRef]
7. Hou, Z.Q.; Duan, L.F.; Lu, Y.J.; Zheng, Y.C.; Zhu, D.C.; Yang, Z.M.; Yang, Z.S.; Wang, B.D.; Pei, Y.R.; Zhao, Z.D.; et al. Lithospheric architecture of the Lhasa Terrane and its control on ore deposits in the Himalayan-Tibetan Orogen. *Econ. Geol.* **2015**, *110*, 1541–1575. [CrossRef]
8. Mole, D.R.; Fiorentini, M.L.; Cassidy, K.F.; Kirkland, C.L.; Thebaud, N.; McCuaig, T.C.; Doublier, M.P.; Duuring, P.; Romano, S.S.; Maas, R.; et al. Crustal evolution, intra-cratonic architecture and the metallogeny of an Archaean craton. *Geol. Soc. Lond. Spec. Publ.* **2015**, *393*, 23–80. [CrossRef]
9. Mole, D.R.; Fiorentini, M.L.; Thebaud, N.; Cassidy, K.F.; McCuaig, T.C.; Kirkland, C.L.; Romano, S.S.; Doublier, M.P.; Belousova, E.A.; Barnes, S.J.; et al. Archean komatiite volcanism controlled by the evolution of early continents. *Proc. Natl. Acad. Sci. USA* **2014**, *111*, 10083–10088. [CrossRef] [PubMed]

10. Wang, C.; Bagas, L.; Lu, Y.; Santosh, M.; Du, B.; McCuaig, T.C. Terrane boundary and spatio-temporal distribution of ore deposits in the Sanjiang Tethyan Orogen: Insights from zircon Hf-isotopic mapping. *Earth-Sci. Rev.* **2016**, *156*, 39–65. [CrossRef]
11. Lu, Y.J.; Wingate, M.T.; Romano, S.S.; Mole, D.R.; Kirkland, C.L.; Kemp, A.I.S.; Belousova, E.A.; Smithies, R.H.; Gessner, K.; Johnson, S.P. Zircon lutetium-hafnium isotope map of Western Australia. *Rec. Geol. Surv. West. Aust.* **2021**, 13–16. [CrossRef]
12. Tilhac, R.; Begg, G.C.; O'Reilly, S.Y.; Griffin, W.L. A global review of Hf-Nd isotopes: New perspectives on the chicken-and-egg problem of ancient mantle signatures. *Chem. Geol.* **2022**, *609*, 121039. [CrossRef]
13. Zahirovic, S.; Seton, M.; Müller, R.D. The Cretaceous and Cenozoic tectonic evolution of Southeast Asia. *Solid Earth* **2014**, *5*, 227–273. [CrossRef]
14. Ma, B.A.W. Precambrian Magmatic Petrogenesis, Metallogenesis and Its Tectonic Setting in the Middle Section of the Western Margin of the Yangtze Block. Doctoral Dissertation, Chengdu University of Technology, Chengdu, China, 2019. (In Chinese)
15. Gao, S.; Qiu, Y.M.; Ling, W.L.; McNaughton, N.J.; Groves, D.I. Single zircon U-Pb dating of the Kongling high-grade metamorphic terrain: Evidence for > 3.2 Ga old continental crust in the Yangtze craton. *Sci. China Ser. D-Earth Sci.* **2001**, *44*, 326–335. [CrossRef]
16. Zheng, Y.F.; Zhang, S.B. Formation and Evolution of Precambrian Continental Crust in South China. *Chin. Sci. Bull.* **2007**, *52*, 1–10. (In Chinese) [CrossRef]
17. Hou, Z.Q.; Zheng, Y.C.; Geng, Y.S. Lithospheric Metal Re-enrichment and Au-Mo-REE Mineralization at Craton Margins. *Miner. Depos.* **2015**, *34*, 641–674. (In Chinese) [CrossRef]
18. Cawood, P.A.; Zhao, G.C.; Yao, J.L.; Wang, W.; Xu, Y.J.; Wang, Y.J. Reconstructing South China in Phanerozoic and Precambrian supercontinents. *Earth-Sci. Rev.* **2017**, *186*, 173–194. [CrossRef]
19. Zhao, X.F.; Zhou, M.F.; Li, J.W.; Selby, D.; Li, X.H.; Qi, L. Sulfide Re-Os and Rb-Sr isotope dating of the Kangdian IOCG metallogenic province, southwest China: Implications for regional metallogenesis. *Econ. Geol.* **2013**, *108*, 1489–1498. [CrossRef]
20. Zhou, M.F.; Zhao, X.F.; Chen, W.T.; Li, X.C.; Wang, W.; Yan, D.P.; Qiu, H.N. Proterozoic Fe–Cu metallogeny and supercontinental cycles of the southwestern Yangtze Block, southern China and northern Vietnam. *Earth-Sci. Rev.* **2014**, *139*, 59–82. [CrossRef]
21. Yang, L.Q.; Deng, J.; Groves, D.I.; He, W.Y.; Li, N.; Zhang, L.; Zhang, R.R.; Zhang, H.R. Metallogenic 'factories' and resultant highly anomalous mineral endowment on the craton margins of China. *Earth Sci. Front.* **2022**, *13*, 101339. [CrossRef]
22. Zheng, Y.F.; Zhao, Z.F. Introduction to the structures and processes of subduction zones. *J. Asian Earth Sci.* **2017**, *146*, 352–366. [CrossRef]
23. Hou, Z.Q.; Yang, Z.M.; Zhang, H.R.; Wang, R.; Song, Y.C.; Liu, Y.; Zheng, Y.C.; Xu, B.; Wang, Q.F.; Liu, Y.C. Continental collision metallogeny: New understandings and progress. *Earth Sci. Front.* **2025**, *32*, 179–209. (In Chinese) [CrossRef]
24. Liu, J.D.; Zhang, C.J.; Liu, X.F.; Li, Y.G.; Yang, Z.X.; Wu, D.C. *Metallogenic Regularities and Prospecting Directions of the Southwestern Margin of the Yangtze Platform*; Geological Publishing House: Beijing, China, 2004; pp. 1–204. (In Chinese)
25. Yin, F.G.; Sun, Z.M.; Wan, F. *Tectonic Evolution and Resource Effects of the Western Margin of the Yangtze Block*; Geological Publishing House: Beijing, China, 2007; pp. 1–158. (In Chinese)
26. Li, X.Y. Crustal Composition and Reconstruction of the Western Margin of the Yangtze Craton: Sr-Nd-Hf Isotope Mapping Constraints of Time Slices. Master's Thesis, China University of Geosciences (Beijing), Beijing, China, 2023. (In Chinese)
27. Gao, X.; Yang, L.Q.; Orovan, E.A. The lithospheric architecture of two subterranes in the eastern Yidun Terrane, East Tethys: Insights from Hf–Nd isotopic mapping. *Gondwana Res.* **2018**, *62*, 127–143. [CrossRef]
28. Wang, C.M.; Bagas, L.; Deng, J.; Dong, M.M. Crustal architecture and its controls on mineralisation in the North China Craton. *Ore Geol. Rev.* **2018**, *98*, 109–125. [CrossRef]
29. Deng, J.; Wang, C.M.; Bagas, L.; Santosh, M.; Yao, E. Crustal architecture and metallogenesis in the south-eastern North China Craton. *Earth-Sci. Rev.* **2018**, *182*, 251–272. [CrossRef]
30. Xu, B.; Hou, Z.Q.; Griffin, W.L.; Zheng, Y.C.; Wang, T.; Guo, Z.; Hou, J.; Santosh, M.; O'Reilly, S.Y. Cenozoic lithospheric architecture and metallogenesis in Southeastern Tibet. *Earth-Sci. Rev.* **2021**, *214*, 103472. [CrossRef]
31. Wang, T.; Huang, H.; Yang, L.Q.; Zheng, Y.C.; Xu, B.; Sun, J.; Hou, T.; Bao, X.W.; Zhang, J.J.; Zhu, X.S.; et al. The methodological framework for deciphering 3-demensional material architecture of the lithosphere. *Acta Geol. Sin.* **2022**, *96*, 3589–3618. (In Chinese) [CrossRef]
32. Yang, L.Q.; He, W.Y.; Gao, X.; Wang, S.R.; Li, N.; Qiu, K.F.; Zhang, L.; Ma, Q.; Su, Y.P.; Li, D.P.; et al. Tracing methods for 3D material architecture of cratonic lithosphere. *Earth Sci. Front.* **2023**, *30*, 391–405. (In Chinese) [CrossRef]
33. Zhao, J.H.; Zhou, M.F.; Yan, D.P.; Zheng, J.P.; Li, J.W. Reappraisal of the ages of Neoproterozoic strata in South China: No connection with the Grenvillian orogeny. *Geology* **2011**, *39*, 299–302. [CrossRef]
34. Wang, X.L.; Zhou, J.C.; Wan, Y.S.; Kitajima, K.K.; Wang, D.; Bonamici, C.; Qiu, S.J.; Sun, T. Magmatic evolution and crustal recycling for Neoproterozoic strongly peraluminous granitoids from southern China: Hf and O isotopes in zircon. *Earth Planet. Sci. Lett.* **2013**, *366*, 71–82. [CrossRef]
35. Wang, W.; Zhou, M.F.; Zhao, X.F.; Chen, W.T.; Yan, D.P. Late Paleoproterozoic to Mesoproterozoic rift successions in SW China: Implication for the Yangtze Block–North Australia–Northwest Laurentia connection in the Columbia supercontinent. *Sediment. Geol.* **2014**, *309*, 33–47. [CrossRef]

36. Zhao, G.C.; Cawood, P.A. Precambrian geology of China. *Precambrian Res.* **2012**, *222–223*, 13–54. [CrossRef]
37. Zhao, J.H.; Li, Q.W.; Liu, H.; Wang, W. Neoproterozoic magmatism in the western and northern margins of the Yangtze Block (South China) controlled by slab subduction and subduction-transform-edge-propagator. *Earth-Sci. Rev.* **2018**, *187*, 1–18. [CrossRef]
38. Zhu, Y.; Lai, S.C.; Qin, J.F.; Zhu, R.Z.; Zhang, F.Y.; Zhang, Z.Z.; Zhao, S.W. Neoproterozoic peraluminous granites in the western margin of the Yangtze Block, South China: Implications for the reworking of mature continental crust. *Precambrian Res.* **2019**, *333*, 105443. [CrossRef]
39. Lai, S.C.; Zhu, Y. Typical Neoproterozoic intermediate-acidic magmatic events and their deep dynamic mechanisms in the western margin of the Yangtze Block: Research progress and prospect. *J. Geomech.* **2020**, *26*, 759–790. (In Chinese) [CrossRef]
40. Fan, H.P.; Zhu, W.G.; Li, Z.X.; Zhong, H.; Bai, Z.J.; He, D.F.; Chen, C.J.; Cao, C.Y. 1.5 Ga mafic magmatism in South China during the break-up of the supercontinent Nuna/Columbia: The Zhuqing Fe-Ti-V oxide ore-bearing mafic intrusions in western Yangtze Block. *Lithos* **2013**, *168*, 85–98. [CrossRef]
41. Wang, Y.J.; Fan, W.M.; Zhang, G.W.; Zhang, Y.H. Phanerozoic tectonics of the South China Block: Key observations and controversies. *Gondwana Res.* **2013**, *23*, 1273–1305. [CrossRef]
42. Wang, Q.F.; Deng, J.; Li, C.S.; Li, G.J.; Yu, L.; Qiao, L. The boundary between the Simao and Yangtze blocks and their locations in Gondwana and Rodinia: Constraints from detrital and inherited zircons. *Gondwana Res.* **2014**, *26*, 438–448. [CrossRef]
43. He, W.Y.; Xing, Y.L.; Bao, X.S.; Sun, N.; Gao, X.; Yang, L.Q. Iron isotope constraints on the genesis of giant Beiya Au-base metal deposits, Yunnan, Southwest China. *Ore Geol. Rev.* **2024**, *171*, 106152. [CrossRef]
44. Chen, W.T.; Zhou, M.F.; Zhao, X.F. Late Paleoproterozoic sedimentary and mafic rocks in the Hekou area, SW China: Implication for the reconstruction of the Yangtze Block in Columbia. *Precambrian Res.* **2013**, *231*, 61–77. [CrossRef]
45. Zhao, X.F.; Zhou, M.F.; Li, J.W.; Sun, M.; Gao, J.F.; Sun, W.H.; Yang, J.H. Late Paleoproterozoic to early Mesoproterozoic Dongchuan Group in Yunnan, SW China: Implications for tectonic evolution of the Yangtze Block. *Precambrian Res.* **2010**, *182*, 57–69. [CrossRef]
46. Yang, H.; Liu, F.L.; Du, L.L.; Liu, P.H.; Wang, F. Zircon U-Pb dating of metamorphic volcanic rocks of the Laochanghe Formation in the Dahongshan Group at the southwestern margin of the Yangtze Block and its geological significance. *Acta Petrol. Sin.* **2012**, *28*, 2994–3014. (In Chinese)
47. Greentree, M.R.; Li, Z.X.; Li, X.H.; Wu, H.C. Late Mesoproterozoic to earliest Neoproterozoic basin record of the Sibao orogenesis in western south China and relationship to the assembly of Rodinia. *Precambrian Res.* **2006**, *151*, 79–100. [CrossRef]
48. Sun, W.H.; Zhou, M.F.; Gao, J.F.; Yang, Y.H.; Zhao, X.F.; Zhao, J.H. Detrital zircon U-Pb geochronological and Lu-Hf isotopic constraints on the Precambrian magmatic and crustal evolution of the western Yangtze Block, SW China. *Precambrian Res.* **2009**, *172*, 99–126. [CrossRef]
49. Zhu, W.G.; Zhong, H.; Li, Z.X.; Bai, Z.J.; Yang, Y.J. SIMS zircon U-Pb ages, geochemistry and Nd-Hf isotopes of ca. 1.0 Ga mafic dykes and volcanic rocks in the Huili area, SW China: Origin and tectonic significance. *Precambrian Res.* **2016**, *273*, 67–89. [CrossRef]
50. Wang, Y.J.; Zhu, W.G.; Huang, H.Q.; Zhong, H.; Bai, Z.J.; Fan, H.P. Ca. 1.04 Ga hot Grenville granites in the western Yangtze block, Southwest China. *Precambrian Res.* **2019**, *328*, 217–234. [CrossRef]
51. Chen, W.T.; Sun, W.H.; Wang, W.; Zhao, J.H.; Zhou, M.F. "Grenvillian" intra-plate mafic magmatism in the southwestern Yangtze Block, SW China. *Precambrian Res.* **2014**, *242*, 138–153. [CrossRef]
52. Chen, W.T.; Sun, W.H.; Zhou, M.F.; Wang, W. Ca. 1050 Ma intracontinental rift-related A-type felsic rocks in the southwestern Yangtze Block, South China. *Precambrian Res.* **2018**, *309*, 22–44. [CrossRef]
53. Zhu, Y.; Lai, S.C.; Qin, J.F.; Zhu, R.Z.; Zhang, F.Y.; Zhang, Z.Z. Petrogenesis and geochemical diversity of late Mesoproterozoic S-type granites in the western Yangtze Block, South China: Co-entrainment of peritectic selective phases and accessory minerals. *Lithos* **2020**, *352–353*, 105326. [CrossRef]
54. Li, X.H.; Li, Z.J.; Ge, W.C.; Zhou, H.W.; Li, W.X.; Liu, Y.; Wingate, M.T.D. Neoproterozoic granitoids in South China: Crustal melting above a mantle plume at ca. 825 Ma? *Precambrian Res.* **2003**, *122*, 45–83. [CrossRef]
55. Sun, W.H.; Zhou, M.F. The ~860-Ma, Cordilleran-type Guandaoshan dioritic pluton in the Yangtze Block, SW China: Implications for the origin of Neoproterozoic magmatism. *J. Geol.* **2008**, *116*, 238–253. [CrossRef]
56. Sun, W.H.; Zhou, M.F.; Yan, D.P.; Li, J.W.; Ma, Y.X. Provenance and tectonic setting of the Neoproterozoic Yanbian group, western Yangtze Block (SW China). *Precambrian Res.* **2008**, *167*, 213–236. [CrossRef]
57. Du, L.L.; Guo, J.H.; Nutman, A.P.; Wyman, D.; Geng, Y.S.; Yang, C.H.; Liu, F.L.; Ren, L.D.; Zhou, X.W. Implications for Rodinia reconstructions for the initiation of Neoproterozoic subduction at ~860 Ma on the western margin of the Yangtze Block: Evidence from the Guandaoshan Pluton. *Lithos* **2014**, *196–197*, 67–82. [CrossRef]
58. Zhu, Y.; Lai, S.C.; Qin, J.F.; Zhu, R.Z.; Liu, M.; Zhang, F.Y.; Zhang, Z.Z.; Yang, H. Neoproterozoic metasomatized mantle beneath the western yangtze block, south china: Evidence from whole-rock geochemistry and zircon u-pb-hf isotopes of mafic rocks. *J. Asian Earth Sci.* **2021**, *206*, 104616. [CrossRef]

59. Geng, Y.S.; Yang, C.H.; Wang, X.S.; Du, L.L.; Ren, L.D.; Zhou, X.W. *Evolution of the Metamorphic Basement at the Western Margin of the Yangtze Platform*; Geological Publishing House: Beijing, China, 2008; pp. 1–215. (In Chinese)
60. Zhuo, J.W.; Jiang, X.S.; Wang, J.; Cui, X.Z.; Xiong, G.Q.; Lu, J.Z.; Liu, J.H.; Ma, M.Z. Initiation time and filling style of the Neoproterozoic Kangdian rift basin at the western margin of the South China Yangtze ancient continent. *Sci. China Earth Sci.* **2013**, *43*, 1952–1963. (In Chinese)
61. Pan, G.T.; Lu, S.N.; Xiao, Q.H.; Zhang, K.X.; Yin, F.G.; Hao, G.J.; Luo, M.S.; Ren, F.; Yuan, S.H. Division and evolution of tectonic stages in China. *Earth Sci. Front.* **2016**, *23*, 1–23. (In Chinese) [CrossRef]
62. Qi, C.J. Geological characteristics and metallogenic model discussion of the Leipu Kahahalo phosphate deposit in southwestern Sichuan. *Geol. Chem. Miner.* **2014**, *36*, 94–100. (In Chinese)
63. Hu, R.Z. *Intracontinental Metallogeny of the South China Block*; Science Press: Beijing, China, 2015; pp. 1–912. (In Chinese)
64. Cheng, J.K. Study on geological structural evolution and mineralization in Jinping Mountain area of Sichuan. *World Nonferrous Met.* **2020**, *24*, 99–100. (In Chinese) [CrossRef]
65. Hu, R.Z.; Fu, S.L.; Huang, Y.; Zhou, M.F.; Fu, S.H.; Zhao, C.H.; Wang, X.J.; Bi, X.W.; Xiao, J.F. The giant South China Mesozoic low-temperature metallogenic domain: Reviews and a new geodynamic model. *J. Asian Earth Sci.* **2017**, *137*, 9–34. [CrossRef]
66. Cai, Y.; Wang, Y.; Cawood, P.A.; Zhang, Y.; Zhang, A. Neoproterozoic crustal growth of the Southern Yangtze Block: Geochemical and zircon U–Pb geochronological and Lu-Hf isotopic evidence of Neoproterozoic diorite from the Ailaoshan zone. *Precambrian Res.* **2015**, *266*, 137–149. [CrossRef]
67. Chen, Q.; Sun, M.; Long, X.P.; Yuan, C. Petrogenesis of neoproterozoic adakitic tonalites and high-k granites in the eastern songpan-ganze fold belt and implications for the tectonic evolution of the western yangtze block. *Precambrian Res.* **2015**, *270*, 181–203. [CrossRef]
68. Meng, E.; Liu, F.L.; Du, L.L.; Liu, P.H.; Liu, J.H. Petrogenesis and tectonic significance of the baoxing granitic and mafic intrusions, southwestern china: Evidence from zircon u–pb dating and lu–hf isotopes, and whole-rock geochemistry. *Gondwana Res.* **2015**, *28*, 800–815. [CrossRef]
69. Wang, Y.J.; Zhou, Y.Z.; Cai, Y.F.; Liu, H.C.; Zhang, Y.Z.; Fan, W.M. Geochronological and geochemical constraints on the petrogenesis of the ailaoshan granitic and migmatite rocks and its implications on neoproterozoic subduction along the sw yangtze block. *Precambrian Res.* **2016**, *283*, 106–124. [CrossRef]
70. Liu, Z.; Tan, S.C.; He, X.H.; Wang, D.B.; Gao, B. Petrogenesis of mid-neoproterozoic (ca. 750 ma) mafic and felsic intrusions in the ailao shan–red river belt: Geochemical constraints on the paleogeographic position of the south china block. *Lithosphere* **2019**, *11*, 348–364. [CrossRef]
71. Zhu, Y.; Lai, S.C.; Qin, J.F.; Zhu, R.Z.; Zhang, F.Y.; Zhang, Z.Z.; Gan, B.P. Petrogenesis and geodynamic implications of neoproterozoic gabbro-diorites, adakitic granites, and a-type granites in the southwestern margin of the yangtze block, south china. *J. Asian Earth Sci.* **2019**, *183*, 103977. [CrossRef]
72. Hu, P.Y.; Zhai, Q.G.; Wang, J.; Tang, Y.; Ren, G.M.; Zhu, Z.C.; Wang, W.; Wu, H. U–pb zircon geochronology, geochemistry, and Sr-Nd-Hf–o isotopic study of middle neoproterozoic magmatic rocks in the kangdian rift, south china: Slab rollback and backarc extension at the northwestern edge of the rodinia. *Precambrian Res.* **2020**, *347*, 105863. [CrossRef]
73. Qi, H.; Zhao, J.H. Petrogenesis of the neoproterozoic low-δ18o granitoids at the western margin of the yangtze block in south china. *Precambrian Res.* **2020**, *351*, 105953. [CrossRef]
74. Zhu, Y.; Lai, S.C.; Qin, J.F.; Zhu, R.Z.; Liu, M.; Zhang, F.Y.; Zhang, Z.Z.; Yang, H. Genesis of ca. 850–835 ma high-mg# diorites in the western yangtze block, south china: Implications for mantle metasomatism under the subduction process. *Precambrian Res.* **2020**, *343*, 105738. [CrossRef]
75. Zou, H.; Bagas, L.; Li, X.Y.; Liu, H.; Jiang, X.W.; Li, Y. Origin and evolution of the neoproterozoic dengganping granitic complex in the western margin of the yangtze block, sw china: Implications for breakup of rodina supercontinent. *Lithos* **2020**, *370–371*, 105602. [CrossRef]
76. Zou, H.; Li, Q.L.; Bagas, L.; Wang, X.C.; Chen, A.Q.; Li, X.H. A neoproterozoic low-δ18o magmatic ring around south china: Implications for configuration and breakup of rodinia supercontinent. *Earth Planet. Sci. Lett.* **2021**, *575*, 117196. [CrossRef]
77. Frisch, W.; Meschede, M.; Blakey, R.C. *Plate Tectonics*; Springer: Berlin/Heidelberg, Germany, 2011.
78. Kemp, A.I.S.; Hawkesworth, C.J.; Paterson, B.A.; Kinny, P.D. Episodic growth of the Gondwana supercontinent from hafnium and oxygen isotopes in zircon. *Nature* **2006**, *439*, 580–583. [CrossRef] [PubMed]
79. Griffin, W.L.; Wang, X.; Jackson, S.E.; Pearson, N.J.; O'Reilly, S.Y.; Xu, X.; Zhou, X. Zircon chemistry and magma mixing, SE China: In-situ analysis of Hf isotopes, Tonglu and Pingtan igneous complexes. *Lithos* **2002**, *61*, 237–269. [CrossRef]
80. Wu, F.Y.; Li, X.H.; Yang, J.H.; Zheng, Y.F. Several issues on the genesis of granites. *Acta Petrol. Sin.* **2007**, *23*, 1217–1238. (In Chinese) [CrossRef]
81. Bennett, V.C.; DePaolo, D.J. Proterozoic crustal history of the western United States as determined by neodymium isotopic mapping. *Geol. Soc. Am. Bull.* **1987**, *99*, 674–685. [CrossRef]

82. Schoene, B.; Dudas, F.O.; Bowring, S.A.; De Wit, M. Sm–Nd isotopic mapping of lithospheric growth and stabilization in the eastern Kaapvaal craton. *Terra Nova* **2009**, *21*, 219–228. [CrossRef]
83. Xu, B.; Hou, Z.Q.; Griffin, W.L.; Yu, J.X.; Long, T.; Zhao, Y.; Wang, T.; Fu, B.; Belousova, E.; O'Reilly, S.Y. Apatite halogens and Sr-O and zircon Hf-O isotopes: Recycled volatiles in Jurassic porphyry ore systems in southern Tibet. *Chem. Geol.* **2022**, *605*, 120924. [CrossRef]
84. Zhang, Z.Y.; Hou, Z.Q.; Pan, X.F.; Fan, X.K.; Zhang, X.W.; Wang, C.G.; Zhang, H.J.; Zhang, K. Crustal accretion, polygenetic reworking, and extensive porphyry-skarn Cu-Au/Fe and W-Mo mineralization: A case study from the central Yangtze River ore belt and adjacent areas, eastern China. *Sci. China Earth Sci.* **2025**, *55*, 1766–1791. (In Chinese) [CrossRef]
85. Mole, D.R.; Frieman, B.M.; Thurston, P.C.; Marsh, J.H.; Jørgensen, T.R.C.; Stern, R.A.; Martin, L.A.J.; Lu, Y.J.; Gibson, H.L. Crustal architecture of the south-east Superior Craton and controls on mineral systems. *Ore Geol. Rev.* **2022**, *148*, 105017. [CrossRef]
86. Wang, T.; Xiao, W.J.; Collins, W.J.; Tong, Y.; Hou, Z.Q.; Huang, H.; Wang, X.X.; Lin, S.F.; Seltmann, R.; Wang, C.Y.; et al. Quantitative characterization of orogens through isotopic mapping. *Commun. Earth Environ.* **2023**, *4*, 110. [CrossRef]
87. Zhang, Z.Y.; Hou, Z.Q.; Lü, Q.T.; Zhang, X.W.; Pan, X.F.; Fan, X.K.; Zhang, Y.Q.; Wang, C.G.; Lü, Y.J. Crustal architectural controls on critical metal ore systems in South China based on Hf isotopic mapping. *Geology* **2023**, *51*, 738–742. [CrossRef]
88. Rudnick, R.L.; Gao, S. Composition of the continental crust. In *Treatise on Geochemistry*; Heinrich, D.H., Turekian, K.K., Eds.; Pergamon: Oxford, UK, 2003; pp. 1–64.
89. Chen, Y.; Xu, Y.G.; Xu, T.; Si, S.K.; Liang, X.; Tian, X.F.; Tian, X.B.; Deng, Y.F.; Chen, L.; Wang, P.; et al. Magmatic underplating and crustal growth in the Emeishan large igneous province, SW China, revealed by a passive seismic experiment. *Earth Planet. Sci. Lett.* **2015**, *432*, 103–114. [CrossRef]
90. Xu, T.; Zhang, Z.J.; Liu, B.F.; Chen, Y.; Zhang, M.H.; Tian, X.B.; Xu, Y.G.; Teng, J.W. Crustal velocity structure in the Emeishan large igneous province and evidence of the Permian mantle plume activity. *Sci. China Earth Sci.* **2015**, *58*, 1133–1147. [CrossRef]
91. Hou, Z.Q.; Zheng, Y.C.; Lu, Z.W.; Xu, B.; Wang, C.M.; Zhang, H.R. Growth, thickening and evolution of the thickened crust of the Tibet Plateau. *Acta Geol. Sin.* **2020**, *94*, 2797–2815. (In Chinese) [CrossRef]
92. Zheng, Y.F.; Chen, Y.X.; Chen, R.X.; Dai, L.Q. Tectonic evolution of convergent plate margins and its geological effects. *Sci. China Earth Sci.* **2022**, *52*, 1213–1242. (In Chinese) [CrossRef]
93. Yang, D.; Lü, Q.T.; Yang, Z.S.; Yan, J.Y.; Xiong, X.; Chen, Y.X. Zircon Hf-isotopic mapping of Middle-Lower Yangtze River Valley Metallogenic Belt, China: Constraints on crustal properties and ore cluster formation. *Lithos* **2021**, *406–407*, 106526. [CrossRef]
94. Belousova, E.A.; Kostitsyn, Y.A.; Griffin, W.L.; Begg, G.C.; O'Reilly, S.Y.; Pearson, N.J. The growth of the continental crust: Constraints from zircon Hf-isotope data. *Lithos* **2010**, *119*, 457–466. [CrossRef]
95. Zheng, Y.F.; Zhang, S.B.; Zhao, Z.F.; Wu, Y.B.; Li, X.H.; Li, Z.X.; Wu, F.Y. Contrasting zircon Hf and O isotopes in the two episodes of Neoproterozoic granitoids in South China: Implications for growth and reworking of continental crust. *Lithos* **2007**, *96*, 127–150. [CrossRef]
96. Cawood, P.A.; Hawkesworth, C.J. Continental crustal volume, thickness and area, and their geodynamic implications. *Gondwana Res.* **2019**, *66*, 116–125. [CrossRef]
97. Kemp, A.I.S.; Hawkesworth, C.J. Granitic perspectives on the generation and secular evolution of the continental crust. In *Treatise on Geochemistry, Volume 3: The Crust*; Rudnick, R.L., Ed.; Elsevier: Oxford, UK, 2003; pp. 349–410.
98. Champion, D.C.; Huston, D.L. Radiogenic Isotopes, Ore Deposits and Metallogenic Terranes: Novel Approaches Based on Regional Isotopic Maps and the Mineral Systems Concept. *Ore Geol. Rev.* **2016**, *76*, 229–256. [CrossRef]
99. Li, X.H.; Li, W.X.; He, B. Formation of the South China Block and the assembly-breakup of Rodinia supercontinent: Observations, interpretations and tests. *Bull. Mineral. Petrol. Geochem.* **2012**, *31*, 543–559. (In Chinese)
100. Deng, J.; Wang, C.M.; Bagas, L.; Selvaraja, V.; Jeon, H.; Wu, B.; Yang, L.F. Insights into ore genesis of the Jinding Zn–Pb deposit, Yunnan Province, China: Evidence from Zn and in-situ S isotopes. *Ore Geol. Rev.* **2017**, *90*, 943–957. [CrossRef]
101. Zhao, X.F.; Zhou, M.F.; Su, Z.K.; Li, X.C.; Chen, W.T.; Li, J.W. Geology, Geochronology, and Geochemistry of the Dahongshan Fe-Cu-(Au-Ag) Deposit, Southwest China: Implications for the Formation of Iron Oxide Copper-Gold Deposits in Intracratonic Rift Settings. *Econ. Geol.* **2017**, *112*, 603–628. [CrossRef]
102. Chen, W.; Zhao, X.F.; Li, X.C.; Zhou, M.F. Basic characteristics and research progress of iron oxide-copper-gold (IOCG) deposits in China. *Acta Petrol. Sin.* **2019**, *35*, 99–118. (In Chinese) [CrossRef] [PubMed]
103. Xu, J.; Xia, X.P.; Wang, Q.; Spencer, C.J.; Lai, C.K.; Zhang, L. Two magma fractionation paths for continental crust growth: Insights from the adakite-like and normal-arc granites in the Ailaoshan fold belt (SW Yunnan, China). *GSA Bull.* **2022**, *134*, 17. [CrossRef]

Disclaimer/Publisher's Note: The statements, opinions and data contained in all publications are solely those of the individual author(s) and contributor(s) and not of MDPI and/or the editor(s). MDPI and/or the editor(s) disclaim responsibility for any injury to people or property resulting from any ideas, methods, instructions or products referred to in the content.